Gas permeability in rarefied flow conditions for characterization of mineral membrane support

C. Savaro, J.P. Bonnet, M.V. Johansson, Pierre Perrier, Irina Martin Graur, P. Moulin

Gas permeability in rarefied flow conditions for characterization of mineral membrane support

Savaro C.[a], Bonnet J.P.[a,1], M.V. Johansson[b], Perrier P.[b], Graur I.[b], Moulin P.[a]

[a]*Aix Marseille Université, CNRS, Centrale Marseille, M2P2 UMR 7340, Equipe Procédés Membranaires (EPM), Europôle de l'Arbois, BP80, Pavillon Laennec, Hall C, 13545 Aix en Provence Cedex, France*
[b]*Aix Marseille Université, IUSTI, CNRS, UMR 7343, 13453 Marseille Cedex, France*

Abstract

Gas Permeability Measurement Technique (GPMT) has the advantage of being a non-destructive method, which is efficient in characterizing filtration membranes. Ceramic filtration membranes consist of successive layers of micro (support) to nano size (skin) pores. When gas flows through such a small scale structure, the molecular mean free path becomes comparable to the pore size. The Slip flow model, validated to describe the gas transport properties under rarefied flow conditions in a microchannel, is extended to porous media. The porous structure is modeled as a cluster of several identical cylindrical channels. By measuring the pressure drop ΔP at several different mean pressures, the pore radius and the porosity on square tortuosity ratio ϵ/τ^2 of the porous model structure that have the same flow property were estimated.

Keywords: Microporous media, Slip flow, Permeametry, Pore size

Nomenclature

G	Geometric factor (m^{-1})
H	Effective length of hollow fiber (m)
J	Mass flux density ($kg.s^{-1}.m^{-2}$)
K	Hydraulic conductivity (s)
Kn	Knudsen number
L_p	Channel length / Gas path length through the porous media (m)
N	Channel number
P	Gas pressure (Pa)
P_0	Pressure upstream the nozzle (bar)
P_1	Pressure upstream the porous sample (bar)
P_2	Pressure downstream the porous sample (bar)
P_c	Nozzle critical pressure (bar)
P_m	Mean pressure (Pa)

*Corresponding author Dr. J.P. Bonnet: jean-philippe.bonnet@univ-amu.fr Tel.: +33 4 42 90 85 01

Q	Total mass flow rate through porous media (kg.s^{-1})
R_m	Middle radius of the hollow fiber (m)
R_{in}	Internal radius of the hollow fiber (m)
R_{out}	External radius of the hollow fiber (m)
S	Membrane cross-sectional area (m^2)
T	Temperature (K)
U_p	Most probable speed of gas particle (m.s^{-1})
k	Permeability (m^2)
k_∞	Intrinsic permeability (m^2)
q	Total mass flow rate through a single channel (kg.s^{-1})
q'_{Kn}	Slip mass flow rate through channel (kg.s^{-1})
q_{Kn}	Knudsen mass flow rate through channel (kg.s^{-1})
q_{poi}	Poiseuille mass flow rate through channel (kg.s^{-1})
r	Channel radius / Pore characteristic length (m)
v_w	Wall velocity (m.s^{-1})
$\mathcal{R}$	Specific gas constant (J.kg^{-1}.K^{-1})
$\mathcal{R}_u$	Universal gas constant (J.mol^{-1}.K^{-1})
ΔP	Pressure drop (Pa)
β	Klinkenberg factor (Pa)
ϵ	Porosity
γ	Heat capacity ratio
λ	Mean free path (m)
$\mathcal{M}$	Molar mass of the gas (kg.mol^{-1})
μ	Dynamic viscosity (Pa.s)
σ_P	Slip coefficient
τ	Tortuosity

1. Introduction

The characterization of porous media is a research topic that has been studied many times in the past. However, it is constantly evolving due to technological advances and the new potential applications in various industrial sectors: health, food, chemical engineering, micro-nano electronics, etc. In these domains the practical applications of the heterogeneous porous media with micro to nano sized pores, are constantly increasing. For numerous membrane processes, used in industrial sectors, the characterization of small scales porous structures is extremely important. More notably, for microfiltration, ultrafiltration and nanofiltration processes, this characterization is of great interest for these two main actors: for membrane manufacturers to improve quality control and structure optimization; and for users, to relate the separation performance to the structural properties of the membrane. The theoretical and technological advances in these fields require a deeper understanding of the phenomena which govern the flows at the micro-and-nano scales.

Different characterization techniques exist and provide relevant information on the porous structure. Most of them unfortunately are destructive, such as the X-ray tomography, electron microscopy, mercury porosimetry *etc.* Among others, the techniques based on the flows of various liquids in the porous structures are particularly efficient and therefore widely used. Generally, they at least allow measurement of pore sizes and the values of porosity [1, 2, 3]. The shortcoming of the liquid implementation is that the porous sample has to be dried after characterization for its further use. The drying process becomes more difficult when the pore sizes decrease because in this case the capillary forces increase. In certain cases, after characterization with a harmful liquid, for example mercury used in mercury porosimetry, the sample becomes totally unusable.

Gas Permeability Measurement Technique (GPMT) has the advantage of being non-destructive for the porous structure, so a usable membrane can be characterized and remains unaffected. In addition, this technique can be used regardless of the dimensions of a sample. However, the gas flows are more complex to model than the liquid flows, due to their compressibility properties. In addition, as the characteristic size of the porous media becomes to be comparable (or smaller) to the gas molecular mean free path, which can happen even under atmospheric conditions, the continuum description of a flow is no longer valid. In this case the modeling taking into account the molecular structure of a gas [4] has to be implemented. Therefore, when characteristic pore size of a sample is less than 100 μm, the kinetic models considering the molecular nature of a gas have to be used to describe the gas flows in porous media.

Microchannel flow models exist and have been experimentally validated to describe the gas transport properties under rarefied flow conditions [5]. Along with determination of the velocity slip and the accommodation coefficients, this approach allows measurements of pressure, to find the dimensions of the channel where a gas flows. The aim of this work is to extend the modeling validated for microchannels to porous structures in order to find the characteristic flow dimensions.

2. Gas flow model

The study of the flows in porous media requires the definition of a structural model to describe the geometry of the poral space. Porous medium can be modeled in a simple way by a bundle of cylindrical tubes. First, the flow through a single tube is modeled, and then the total flow through porous medium is calculated as the sum of flows through all tubes.

2.1. Gas flow model in microchannel

When the molecular mean free path, λ, becomes comparable to a characteristic dimension of a micro fluidic device, the compressible Navier-Stokes equations start to failure in accurately flow describing due to the rarefaction effects [6, 7, 8, 9, 10]. Therefore, to estimate the limit of applicability of the Navier-Stokes equations the molecular mean free path has to be calculated. It is inversely proportional to the pressure and its value can be slightly different depending on the collision model between particles [7, 8]. Here we have chosen to use a so called equivalent mean free path, where the coefficient due to the collision model is omitted:

$$\lambda = \frac{\mu}{P}\sqrt{2\mathcal{R}T} = \frac{\mu}{P}U_P, \qquad U_P = \sqrt{2\mathcal{R}T}, \tag{1}$$

where T is the gas temperature, μ is the dynamic viscosity, P is the gas pressure, U_P is the most probable molecular speed and $\mathcal{R} = \mathcal{R}_u/\mathcal{M}$ is the gas specific constant, $\mathcal{M}$ is the gas molar mass, and $\mathcal{R}_u$ is the universal gas constant.

When the characteristic length of the channel r is of the order of or smaller than the molecular mean free path, three flow regimes could be important, namely: slip flow, transitional flow and free molecular (Knudsen diffusion) regimes, see definitions below. These regimes are usually classified using the Knudsen number, Kn, defined as the ratio between the molecular mean free path and a characteristic length of the flow, usually the channel radius or diameter [7]:

$$Kn = \frac{\lambda}{r} = \frac{\mu}{rP}\sqrt{2\mathcal{R}T}. \tag{2}$$

All gas flow regimes in a channel can be so classified using the Knudsen number as follow [7, 5]:

Continuum flow, ($Kn < 0.001$): The flow is well described by the Navier-Stokes equations with the classical non-slip boundary conditions for the gas velocity at the walls.

Slip flow, ($0.001 < Kn < 0.1$): The flow can still be described by the Navier-Stokes equations, taking into account the velocity slip and temperature jump boundary conditions at the walls.

Transition flow, ($0.1 < Kn < 10$): In this flow regime the continuum assumptions are not valid anymore. The number of collisions between the molecules becomes comparable to the number of collisions between the molecules and the walls. The flow is described by the Boltzmann equation.

Free molecular flow (Knudsen diffusion), ($Kn > 10$): The collisions of gas molecules with walls largely dominate the collisions between the gas molecules. Therefore, the interactions between the gas molecules can be completely neglected and the flow can be considered as diffusion of a gas, Knudsen diffusion, driven by the gas molecules with walls collisions, and can be described by the Knudsen equation or collisionless Boltzmann equation.

The models corresponding to each of these regimes [6, 7, 11] are validated in the case of a single microchannel with known dimensions [7, 8, 5, 12]. We will focus here on an isothermal, non-inertial and stationary flow in a cylindrical channel of radius r and length L_p. In the continuum flow regime, the mass flow rate through this channel is found by the solution of the Stokes equation, and it is called the Poiseuille mass flow rate:

$$q_{poi} = \frac{\pi r^4}{8\mu\mathcal{R}TL_p}P_m\Delta P, \tag{3}$$

where P_m is the mean pressure, and ΔP is the pressure drop along the channel. It is clear that the Poiseuille mass flow rate q_{poi} is proportional to $P_m\Delta P$. The previous expression is valid only in the hydrodynamic flow regime. In the free molecular flow regime (Knudsen diffusion), the flow is driven by the diffusion mechanism between gas molecules and the channel walls and all interactions between gas molecules are neglected [11]. This phenomenon is called the Knudsen diffusion and the corresponding mass flow rate is proportional only to ΔP:

$$q_{Kn} = \frac{2-\alpha}{\alpha}\frac{8}{3\sqrt{\pi}}\frac{\pi r^3\Delta P}{L_p U_P}, \tag{4}$$

where q_{Kn} is the Knudsen diffusion mass flow rate through a channel, and α is the accommodation coefficient [4], [5]. This expression is valid only in the free molecular flow regime.

As an approximation the mass flow rate between these two regimes can be expressed as the sum of Poiseuille and Knudsen mass flow rates:

$$q = q_{poi} + q_{Kn} = q_{poi}\left(1 + \frac{2-\alpha}{\alpha}\frac{32}{3\sqrt{\pi}}Kn\right). \tag{5}$$

In the previous expression the Knudsen number is calculated using Eq. (2), where P is equal to the mean pressure P_m. As in Eq. (4), the accommodation coefficient α, $0 \leq \alpha \leq 1$, is used to take into account the gas surface interaction and should conform to experiments [13, 14, 15]. Previous expression is very approximate one and it can be used only for very rough estimations of the mass flow rates in all Knudsen number ranges, *i.e.* from continuum to free molecular flow regime. By its construction, this expression provides good approximation only for two limit cases: the continuum flow regime, when $Kn \to 0$ and the free molecular regime, where $Kn \to \infty$.

In all gas flow regimes a thin layer, Knudsen layer, whose thickness is on the order of a few molecular mean free paths, exists near a solid surface. Inside this layer a gas is not in equilibrium, due to the insufficient number of molecule-molecule collisions needed to reach an equilibrium. Therefore, in this layer the gas velocity does not equal to the wall velocity and the slip phenomenon exists. Only the Boltzmann equation can provide the correct description of this phenomenon. However, the use of the Navier-Stokes equations along with the velocity slip boundary conditions allows us to simulate the gas properties adequately in the slip flow regime [4].

The first order velocity slip boundary condition at wall is given by [16]:

$$v_w = \sigma_P \lambda \left.\frac{\partial v}{\partial n}\right|_{wall}, \tag{6}$$

where σ_p is the velocity slip coefficient, v_w is the slip velocity, and n is the direction normal to the wall. Slip velocity is proportional to the slip coefficient σ_p, which characterizes the collisions between the gas molecules and the wall. In the limit case, when all the molecules colliding with a wall are then diffused with a zero mean velocity in an arbitrary direction, the velocity slip coefficient can be calculated theoretically and is equal to $\sigma_P = 1.016$ [4]. If some of incident molecules are reflected specularly, *i.e.* by just reversing the normal components of their velocity to the opposite one, then the slip velocity is naturally higher, so σ_P has larger values. Generally speaking, for a non-polished wall, the velocity slip coefficient is in the range: $1.016 \leq \sigma_P \leq 1.3$ [7, 8].

It should be pointed out that the use of the Navies-Stokes equations subjected to the velocity slip boundary condition, Eq. (**??** is only valid if the Knudsen number is small enough, $Kn \leq 0.1$, *i.e.* that the gas flow is in the slip flow regime. For larger Knudsen numbers the Navier-Stokes equations become invalid and the statistical mechanic approach has to be implemented to simulate the gas flow. In practice, this slip flow approach decreases in precision compared to the numerical solution of the Boltzmann equation when the Knudsen number becomes larger than 0.1, which was confirmed experimentally.

The mass flow rate through a channel, obtained from the analytical solution of the Stokes equation with the velocity slip boundary condition, Eq. (6), reads [17]:

$$q = q_{poi}\left(1 + 4\sigma_P Kn\right). \tag{7}$$

The previous expression can be also interpreted as the sum of a Poiseuille mass flow contribution proportional to $P_m \Delta P$ and a Knudsen mass flow contribution proportional to ΔP, and this sum can be written in a similar form as equation (5):

$$q = \frac{\pi r^4}{8\mu' \mathcal{R} T L_p} P_m \Delta P + \sigma_p \frac{\pi r^3}{L_p U_P} \Delta P = q_{poi} + q'_{Kn}, \tag{8}$$

where q'_{Kn} is the term which has the structure similar to the Knudsen diffusion term, see Eq. (4). It should be noted that in the previous expression, as in Eq. (6), the velocity slip coefficient depends on the accommodation coefficient, which means, on the way of the interaction between the molecules and the walls.

Analysis of equation (8) shows that this flow regime would be particularly convenient for sizing a channel to determine a characteristic dimension of a microchannel, *i.e. its radius.* Indeed, as the Poiseuille mass flow is proportional to r^4 and the Knudsen flow is r^3 dependent, the ratio between these two contributions gives an information on the radius r. By measuring the pressure drop ΔP for several different mean pressures, we can separate these two contributions that are respectively proportional and independent of P_m. In other words, we measure the ratio $q'_{Kn}/q_{poi} = 4\sigma_P Kn = 4\sigma_P r\mu U_P / P_m$ to deduce a characteristic dimension of the channel, *i.e. its radius.* However, the coefficient σ_p introduces some uncertainty, because it is not known for a given pair gas/surface. However, the velocity slip coefficient has a limited theoretical range and the value 1.016 can be considered as a minimum of its possible values.

The previous equations were derived for a channel with a cylindrical cross-section. Generalization for the microchannel with a rectangular cross-section can be found in [18].

The slip regime takes place when the mean free path is about one to three orders of magnitude smaller than the characteristic channel dimension. At 20 °C, the mean free path of nitrogen and argon are on the order of 75 nm at ambient pressure and on the order of 0.75 µm at 100 mbar. To obtain an acceptable precision on the measured characteristic dimension r, it was necessary to work respecting two conditions: on one hand, the Knudsen contribution

has to be significant and, on other hand, the Knudsen number needs to be lower than 0.1 to stay in the slip flow regime. Using equation (8) the Knudsen flow contribution regarding the total flow of nitrogen is calculated for channels with different radius as a function of the mean pressure (Figure 1). It was found that for considered microchannels radius, the adapted pressure range for nitrogen is 0.3 - 5 bar. The mean free path of argon in of the same order of magnitude as that of nitrogen, so the pressure range is the same.

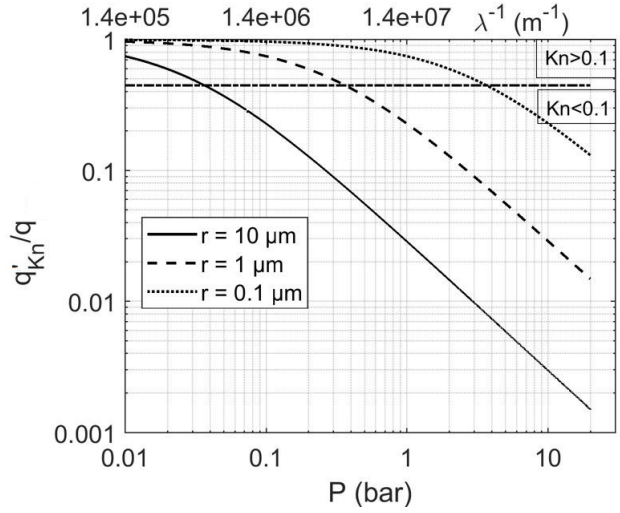

Figure 1: Slip flow regime: variation of Knudsen flow contribution, $q_{Kn'}$, to the total flow, q as a function of pressure, using nitrogen as the working gas, for different channels radius and $\sigma_P = 1.016$. Intercept with the horizontal curve gives the threshold value of the Knudsen number equal to 0.1.

2.2. Extending the slip flow model from microchannel to an idealized porous medium

The flow model previously described for a single narrow tube can be extended to porous medium considering a group of N cylindrical channels with a uniform radius r and a uniform length L_p, distributed over the cross-section S of a parallepipeded volume of thickness L (Figure 2). The characteristic of tortuosity is introduced as pore length, which could be greater than the thickness L. The tortuosity is defined as the ratio between L_P and L: $\tau \equiv L_P/L$. The porosity is defined as the ratio between the pore volume and the total volume: $\epsilon = N\pi r^2 L_p/S\,L$.

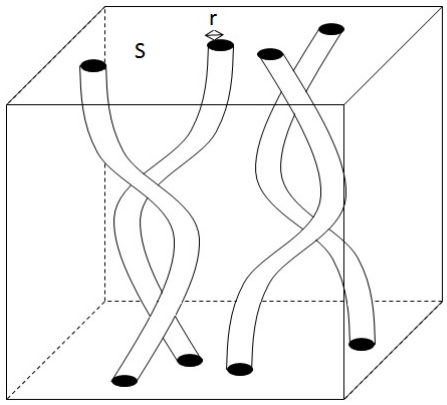

Figure 2: Porous medium modeled as cluster of channels with a unique radius r and a length L_P.

The transport properties of this porous medium are characterized using a Darcy-type law that is typically seen in chemical engineering literature. The hydraulic conductivity K (s) allows to characterize the total mass flow Q in the

porous material and is defined as

$$\frac{Q}{S} = K\frac{\Delta P}{L}. \tag{9}$$

The permeability k (m^2) allows to measure the porous media intrinsic transport properties by excluding the viscosity and density of the flowing fluid

$$\frac{Q}{S} = k\frac{\rho}{\mu}\frac{\Delta P}{L}. \tag{10}$$

From the ideal gas law and the mean free path definition, equation (1), one obtains:

$$\rho = \frac{P}{\mathcal{R}T} \Rightarrow \frac{\rho}{\mu} = \frac{2}{\lambda U_P}. \tag{11}$$

As long as the pressure drop is smaller than de mean pressure, calculate the mean free path based on the mean pressure is an acceptable approximation:

$$\lambda = \frac{\mu}{P_m}U_P \tag{12}$$

Expressing the total mass flow rate Q as the sum of the mass flow rate of each channel and using equations (3), (7) and (11) the hydraulic conductivity K is written as

$$K = \frac{\epsilon r^2}{8\tau^2}\frac{2}{U_P}\left(\frac{1}{\lambda} + \frac{4\sigma_P}{r}\right) \tag{13}$$

and the permeability k is expressed as

$$k = \frac{\epsilon r^2}{8\tau^2}\left(1 + 4\sigma_P Kn\right) = k_\infty\left(1 + \frac{\beta}{P_m}\right). \tag{14}$$

Equation (14) has the same form as the Klinkenberg law [19, 9]. The factor $k_\infty = \epsilon r^2/8\tau^2$ is the permeability of a material at high pressure, *i.e.* when the slip flow impact is negligible and it is called the intrinsic or liquid permeability. As it follows from equation (14) the Klinkenberg factor β is equal to $4\sigma_p\mu U_P/r$. Therefore, it is gas dependent through viscosity slip coefficient, σ_P, gas viscosity, μ, and the most probable velocity, U_P; and also medium dependent through the characteristic dimension of channels, r.

It is worth to underline that as long as the pressure drop for each experiment is far smaller than the mean pressure, then hydraulic conductivity and permeability are only mean pressure dependent.

Usually the external dimensions of porous medium sample, L and S, are known. By performing measurements of the mass flow rate and pressure drop on this sample at various pressure levels, the hydraulic conductivity, eq. (9), can be calculated:

$$K = \frac{Q}{\Delta P}\frac{L}{S}. \tag{15}$$

According to equation (13), KU_p product should follow the law $f(1/\lambda)$:

$$KU_p = \underbrace{\frac{\epsilon r^2}{4\tau^2}}_{a}\frac{1}{\lambda} + \underbrace{\frac{\epsilon r\sigma_p}{\tau^2}}_{b} = a\frac{1}{\lambda} + b. \tag{16}$$

The parameters a and b in eq. (16) can be calculated from the linear regression fit of the experimental data. The slope a and the intercept b are two characteristic properties of the porous sample. From these coefficients the characteristic radius r and the number ϵ/τ^2, which determines the structure properties of the membrane, may be deduced as:

$$r = 4\sigma_p\frac{a}{b} \qquad \text{and} \qquad \frac{\epsilon}{\tau^2} = \frac{1}{4\sigma_p^2}\frac{b^2}{a}. \tag{17}$$

To know the value of σ_P, which characterizes the gas-solid surface interaction for the given sample, additional measurements have to be done. However, the use of $\sigma_P = 1.016$ would give a "minimum" value for the pore radius, in the sense that the real mean radius is probably slightly greater, but it is unlikely smaller. For the same reason ϵ/τ^2 can be interpreted as a "maximum" value. This ratio appears naturally from the theory as a number characterizing the structural properties of the porous sample. It shows that in fact, even a very high porosity material can have a very small permeability if the tortuosity factor is high.

3. Material

3.1. Fluid setup

The Fluid Loop is a classic gas permeameter setup (figure 3). It is made of stainless steel and designed to ensure, and measure, a constant mass flow rate passing through a porous sample at different mean pressures, and over a wide range of flow rates. The porous sample to be characterized is located in a rigid stainless steel cartridge and connected between two tanks of volumes V_1 and V_2. The pressure drop ΔP is measured between the inlet (V_1) and outlet (V_2) tanks, $\Delta P = P_1 - P_2$. The acquisition of all sensor signals (differential pressure, absolute pressure and temperature) is done simultaneously with the same frequency. The vacuum pump is switched on to empty all the fluid loop until

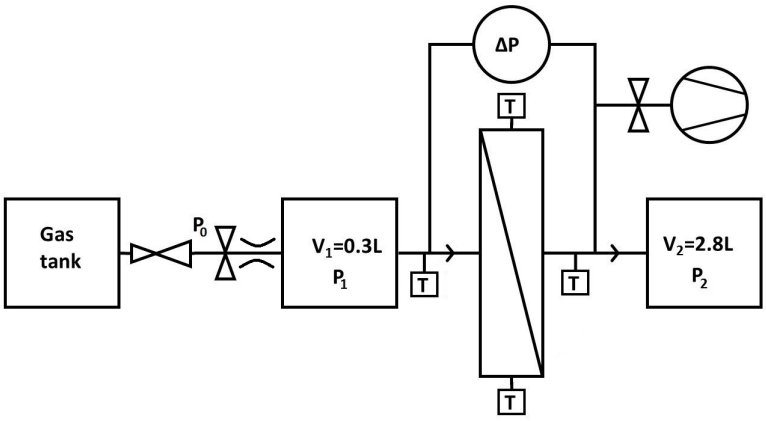

Figure 3: Schematic diagram of the experimental setup.

pressure is less than 3 mbar. The absence of leakage after stopping the vacuum pump is verified by following the temporary evolution of the pressure signals. A constant pressure 5 bar $< P_0 <$ 15 bar is applied upstream of a sonic nozzle using a pressure regulator. This ensures the fluid loop fills up at a constant mass flow rate that depends on the nozzle aperture, temperature and P_0. The experiment starts when the valve, located after the pressure regulator, is opened. The mass flow rate should stay constant as long as the downstream pressure P_1 is below the critical pressure $P_c = P_0(\frac{2}{\gamma+1})^{\frac{\gamma}{\gamma-1}}$, where γ is the heat capacity ratio of the gas used in the experiment [20]. The critical pressure P_c for Nitrogen and Argon is equal to $0.53P_0$ and $0.49P_0$, respectively. Various Bird precision® nozzles with a wide range of apertures sizes ranging from 0.05 mm to 0.737 mm were used to cover over 3 order of magnitude of mass flow rates, from 10^{-6} kg s^{-1} to 10^{-3} kg s^{-1}.

Figure 4 shows an example of a raw data of pressure variation in time. The variations of pressures P_1 and P_2 are measured by Keller® absolute piezoresistive sensors (accuracy of $\delta(P) = 3$ mbar), see Figure 4(a). Pressure difference, ΔP, is measured by a Rosemount® differential pressure sensor (accuracy of $\delta(\Delta P) = 0.05$ mbar), see Figure 4(b). The acquisition is started a few seconds before opening the inlet valve, the opening time is about 1/2 s. Typically, ΔP increases to a maximum value relatively rapidly, in $10 - 20$ seconds, then slowly decreases to return to zero at infinite time. Data on ΔP variation before t_0, *i.e.* before ΔP reaches its maximum, are removed from the analysis. The data at the end of experiments where $\delta(\Delta P)/\Delta P < 1\%$ are also removed to insure a sufficient precision. Most of the time the experiments are stopped before the pressure reached P_0, because it is clear that at this time the relevant data are already recorded.

All experiments were performed at room temperature. Four thermocouples are placed at various locations in the system to monitor the temperature variations (Figure 5). From the temperature measurement analysis it is clear that the temperature varies very slightly during the experiment.

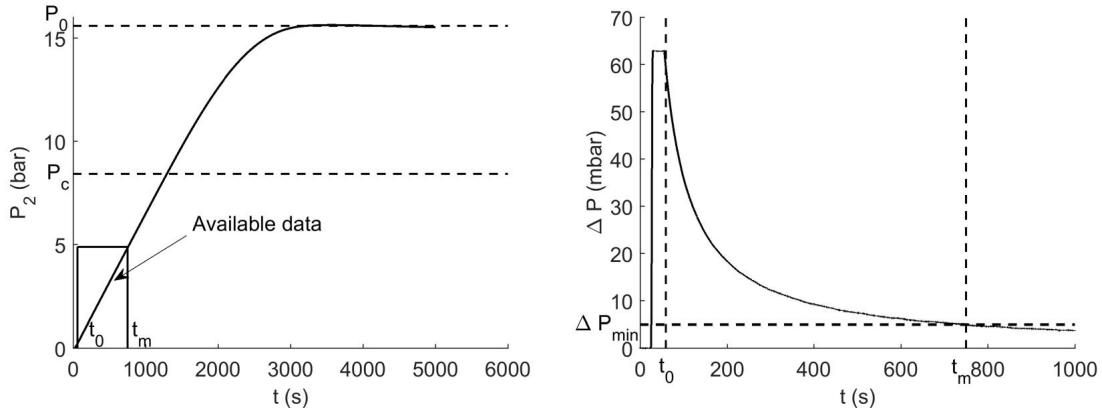

Figure 4: Raw pressure measurement during an experiment: (a) Pressure vs. time, (b) Pressure difference (upstream and downstream the membrane) vs. time.

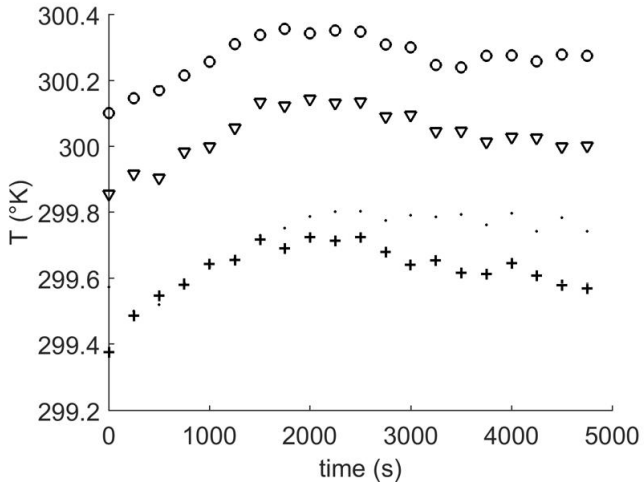

Figure 5: Temperature measurement from the different sensors vs. time.

The molar flow rate $Q/\mathcal{M}$ through the membrane is calculated using the ideal gas law in the outlet tank of the volume V_2 [8]:

$$\frac{Q}{\mathcal{M}} = \frac{V_2}{\mathcal{R}_u T}\frac{d(P_2)}{dt}\left(1 - \frac{dT/T}{dP_2/P_2}\right), \tag{18}$$

The nozzle sets and maintains a flow rate allowing the increase of pressure in the volume V_2 to stay slow enough that the gas remains at the room temperature: its temperature did not vary more than 1 °C for the duration of the experiments. The relative variation of the temperature during the experiment, dT/T, was of the order of 10^{-2}, so that it was negligible against the relative variation of pressure dP/P that is of the order of 1. Therefore Equation (18) may be simplified as:

$$Q = \frac{V_2}{\mathcal{R}T}\frac{dP_2}{dt}. \tag{19}$$

The derivative dP_2/dt is calculated using a Savitzky-Golay filter with a correlation time such that P_2 rises in $dP = 0.15$ bar during this time period, so that the uncertainty for the pressure increase remains smaller than $\delta P/dP = 2\%$. This time is calculated by a rough linear estimation of the mass flow rate, which ensures that $\delta P/dP < 3\times10^{-3}/0.15 = 2\%$. The uncertainty on the volume measurement of the outlet tank, V_2, is 2%. Thus the mass flow rate uncertainty is:

$$\frac{\delta Q}{Q} = \frac{\delta V}{V_2} + \frac{\delta T}{T} \quad + \frac{\delta t}{dt} + \frac{\delta P}{dP}, \tag{20}$$
$$\frac{\delta Q}{Q} = 2\% + 0.05\% + 1\% + 2\% = 5\%.$$

If the pressure drop across the porous sample is small enough compared to the mean pressure within the porous sample, the mass flow rate that passes through the sample is the same as the constant flow rate passing through the nozzle [21]. Figure 6 shows the mass flow rate measured in V_2 during various experiments confirming this behavior. For the data analysis, the points with $P/P_0 > P_c/P_0$ were systematically rejected, because for the higher values of the ratio P/P_0 the mass flow rate begins to decrease, see Figure 6.

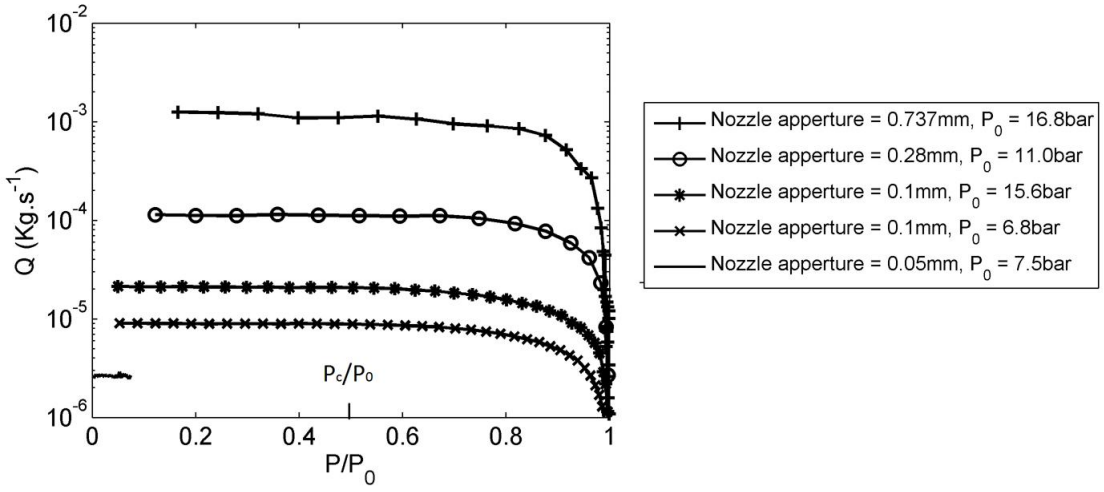

Figure 6: Variation of mass flow rate Q in [kg s^{-1}] vs. dimensionless pressure, P/P_0, for different nozzle apertures and different upstream pressures. The mass flow rate remains reasonably constant for $P < P_c$.

3.2. Sample: ceramic support for ultra/nano filtration membrane

Measurements were performed on several ceramic hollow fibers, designed and manufactured by Tami industry®. This porous matter is commonly used as a support in the ceramic membranes field: the active layer is deposited on this type of porous material. Hollow fibers are 29 cm long made of homogeneous porous ceramic material with internal radius $R_{in} = 0.85$ mm and external radius $R_{out} = 2.10$ mm. Both ends of a fiber are sealed over 1 cm to adapt them to the cartridge and to force the entire mass flow to cross the porous medium from the inside to the outside of the pipe (Figure 7), therefore the effective length of this support is $H = 27$ cm. Historically, for this kind of ceramic support, the manufacturer uses the Mercury Porosimetry to characterize it. Slightly dependent on the production batch, the mercury porosimetry technique results provided by the manufactures for this type of materials, show a typical pore size around $r = 2.2$ µm and a porosity around $\epsilon = 25\%$.

The tubular shape of the support introduces a difficulty to properly define the effective surface S, but was accomplished by the following. Considering a small slice dR of the tube radius R and supposing for each slice the validity of

*Manufacturer data

Table 1: Characteristic of the hollow fiber.

Internal radius, R_{in}	0.85 mm
External radius, R_{out}	2.10 mm
Total length	290 mm
Sealing (both ends)	10 mm PTFE
Porosity	$\sim 25\%$
Pore radius *	1.5-3 µm

Figure 7: Picture of a hollow fiber.

definition (15), assuming then that dP is the pressure drop through a slice and that the flow rate is the same for each slices, one obtains:

$$K = \frac{Q}{dP}\frac{dR}{2\pi RH}. \tag{21}$$

The pressure drop through a slice dR can be expressed as:

$$dP = \frac{Q}{2\pi KH}\frac{dR}{R}. \tag{22}$$

Therefore the relation between the total pressure drop, ΔP, and the hydraulic conductivity, K, is obtained by integration over dP:

$$\Delta P = \int_{R_{in}}^{R_{out}} dP = \int_{R_{in}}^{R_{out}} \frac{Q}{2\pi KH}\frac{dR}{R} = \frac{Q}{K}\frac{1}{2\pi H}\ln\frac{R_{out}}{R_{in}} = \frac{Q}{K}G. \tag{23}$$

As the hydraulic conductivity K is pressure dependent, and pressure is radius dependent, so K is also radius dependent. Nevertheless, as long as experimental conditions ensure pressure drop to be far smaller than the mean pressure, so the hydraulic conductivity could be considered as radius independent and therefore put outside the integral in Eq. (23). From relation (23) the tube hydraulic conductivity is expressed as

$$K = \frac{Q}{\Delta P}G, \tag{24}$$

where

$$G = \frac{1}{2\pi H}\ln\frac{R_{out}}{R_{in}} \tag{25}$$

is a geometrical factor that covers up the porous media dimensions. From Eq. (24) the tube hydraulic conductivity can be expressed as:

$$K = \frac{Q}{\pi H\Delta P}\frac{1}{2}\ln\frac{1+A}{1-A}, \qquad A = \frac{R_{out}-R_{in}}{R_{in}+R_{out}}. \tag{26}$$

When $|A| < 1$ we can transform the previous expression in the following:

$$K = \frac{Q}{\pi H\Delta P}\operatorname{artanh} A = \frac{Q}{\pi H\Delta P}\operatorname{artanh}\frac{\Delta R}{2R_m}, \tag{27}$$

where $\Delta R = R_{out} - R_{in}$ is the membrane thickness and $R_m = (R_{in} + R_{out})/2$ is the middle radius of the tube. In the small curvature limit, *i.e.* $\Delta R \ll R_m$, the value of A, Eq. (26), is small compared to 1 ($A \ll 1$), so $\operatorname{artanh}(A) \approx A$, then

$$K = \frac{Q}{\Delta P}\frac{\Delta R}{2\pi H R_m} = \frac{Q}{\Delta P}\frac{\Delta R}{S}, \tag{28}$$

and we naturally recover $G \approx \Delta R/S$, where $S = 2\pi R_m H$ is the middle surface. In our case $G = 0.5331$ m^{-1} and $\Delta R/S = 0.4995$ m^{-1}, so they differ by 7%, therefore the curvature effects are small but still significant. In the following the mass flux $J = Q/S$ is calculated using this definition of S as $2\pi R_m H$.

4. Results

4.1. Detailed results for one porous hollow fiber sample

The model, developed in Section 2.2, needs to be experimentally confirmed. Indeed, several strong assumptions have been made, especially concerning the shape of the porous structure. To validate these assumptions different experiments were performed. Several parameters were varied such as the mass flow rate, its direction and the nature of the gas. Special attention was paid to the repeatability of the measurement after removing the membrane from the cartridge. The results of these experimental studies are discussed below.

The characteristic curves, as defined in equation (16), for the same hollow fiber at various mass flow rates are shown in Figure 8(a). The curves are linear, as expected by the model, and they gather on the same straight line, except for the data obtained with the greater flow rate that are slightly offset. By analyzing the determination coefficient, R^2, see Figure 8(b), it is evident that this coefficient decreases drastically for mass flows greater than 2×10^{-2} kg s^{-1} m^{-2} (Figure 8(b)). The coefficients a and b calculated with a linear regression for each mass flow rate are shown in Figure 9. The slope a and intercept b start to vary significantly for mass flows higher than $J \approx 2\text{-}5 \times 10^{-2}$ kg s^{-1} m^{-2} (Figure 9).

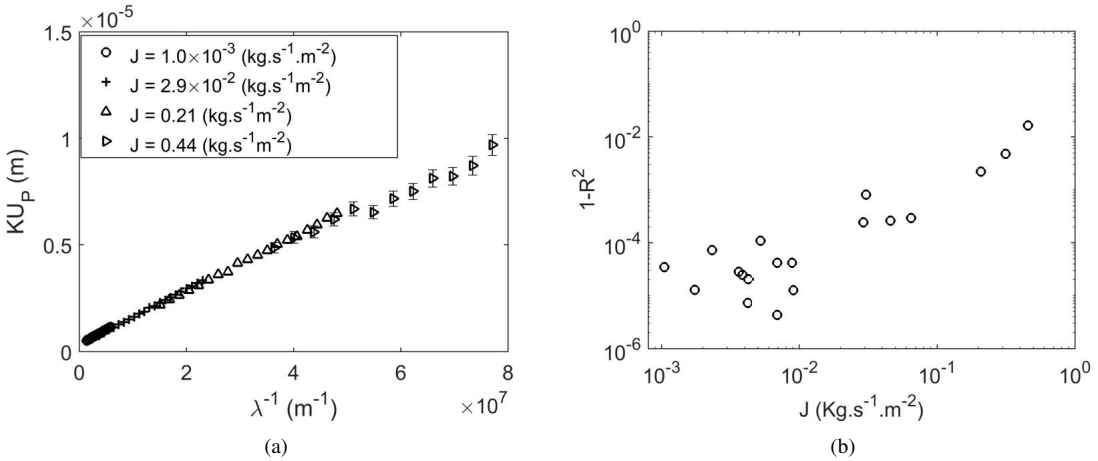

Figure 8: (a) Variation of KU_P as a function of the inverse mean free path for different mass flow rates. (b) Variation of expression $(1 - R^2)$, where R^2 is the determination coefficient of the linear regression, as a function of mass flow rate.

The impact of the intensity of the mass flow rate on the linear fit quality can be interpreted as the threshold of the appearance of inertial effects, which are not that easy to predict [22]. This threshold should not vary much for similar porous media and under the same operating conditions. Therefore, the flows are limited to 5×10^{-3} kg s^{-1} m^{-2}. At least two measurements, at significantly different flow rates, were taken for each sample to verify that the slope and intercept did not vary significantly.

As described in Section 3.2, the hollow fiber is set in a stainless steel cartridge and is sealed by 2 viton seals located at each end of the fiber. The relative position of the membrane versus the cartridge may change slightly after each

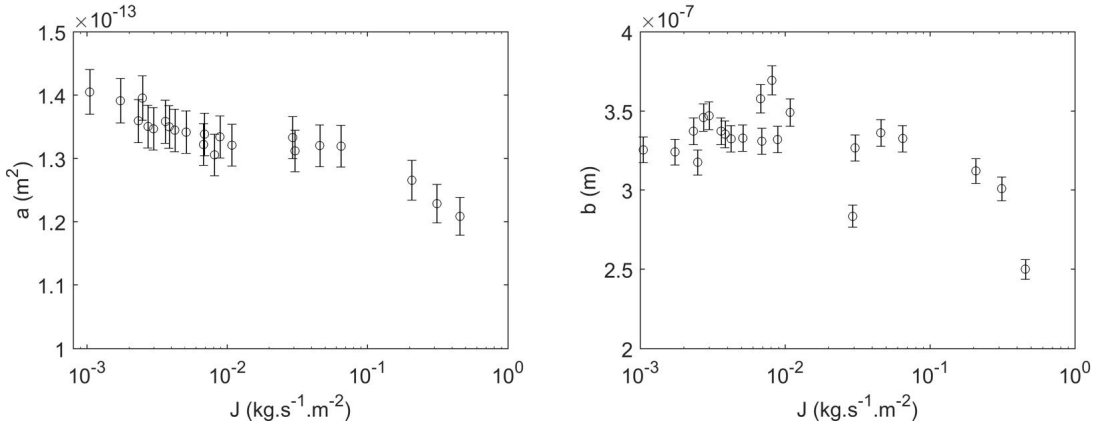

Figure 9: Coefficients of the fitting curve, eq. (16), calculated with linear regression as a function of the mass flow rate: (a) a coefficient data, (b) b coefficient data.

assembly. To evaluate the impact of the membrane assembly, the measurements were made before and after assembly of the fiber in the cartridge. No difference was found between the flow characteristics before and after disassembly (Figure 10(a)). This behavior assures the repeatability of the proposed method. Small deviations are observed when the gas flow direction is inverted, but they are of the order of the measurement accuracy (Figure 10(b)).

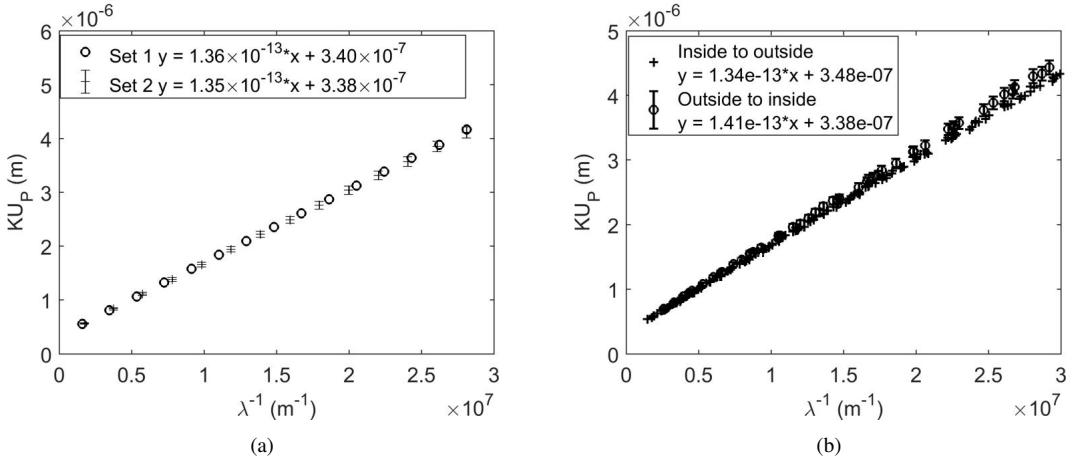

Figure 10: Variation of KU_P as a function of the inverse mean free path for: (a) different sets of the same membranes in the cartridge; (b) different flow directions.

The data of permeability K as a function of pressure are reported on Figure 11(a) for both argon and nitrogen. It is clear that the curves for the two gases have different slopes. Nevertheless, when the same permeability data, but multiplied by the most probable velocity, U_P, are plotted as a function of inverse molecular mean free path, then the data are gathered on the same unique curve that characterizes the porous sample (Figure 11(b)). Therefore, the nature of a gas, used to characterize the porous, sample does not show visible impact on the determination of r and ϵ/τ^2.

Furthermore, a controlled addition of glue to the support to extend the sealing surface confirmed that the sealing does not bring unpredicted complications and the change of the active surface is taken into account properly.

All experiments were carried out at room temperature 23 ± 2 °C and no impact on the characteristic curve was observed for a temperature variation of the order of 5 °C.

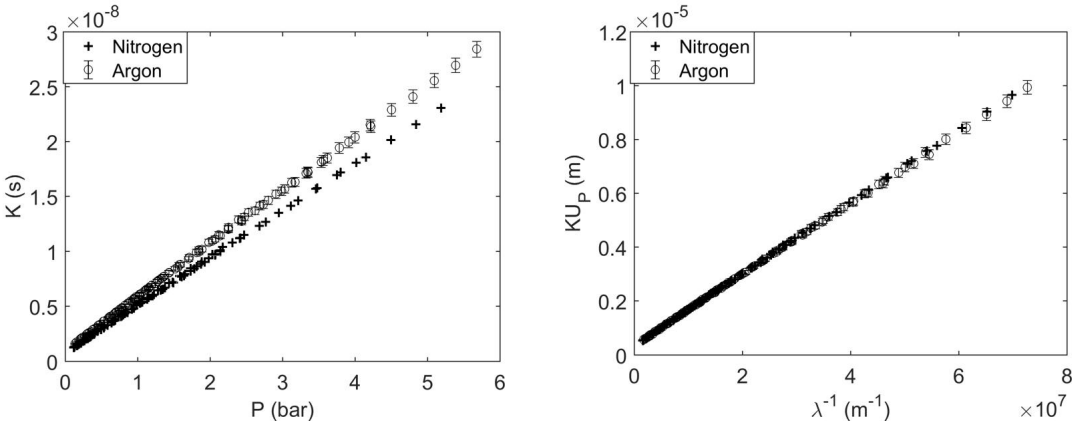

(a) (b)

Figure 11: Measurement of the same hollow fiber with different gases (a)Variation of K as a function of the absolute pressure. (b) Variation of KU_P as a function of the inverse mean free path.

4.2. Measurements on various similar hollow fiber

Different microporous ceramic samples (S10, S20, S30 and S31) from three different manufacturing batches were characterized by the proposed method (S30 and S31 come from the same batch). The manufacturing process remains the same, however, operating parameters and the quality of the raw material may vary slightly from one batch to another (Tami industry®). $KU_P = f(1/\lambda)$ data are plotted on Figure 12 for four porous hollow fibers. All the samples present distinct results which constitute a single signature for each of them. For each sample KU_P varies linearly with $1/\lambda$. The linear regression coefficients a and b, the pore radius, r, and the structure property coefficient,

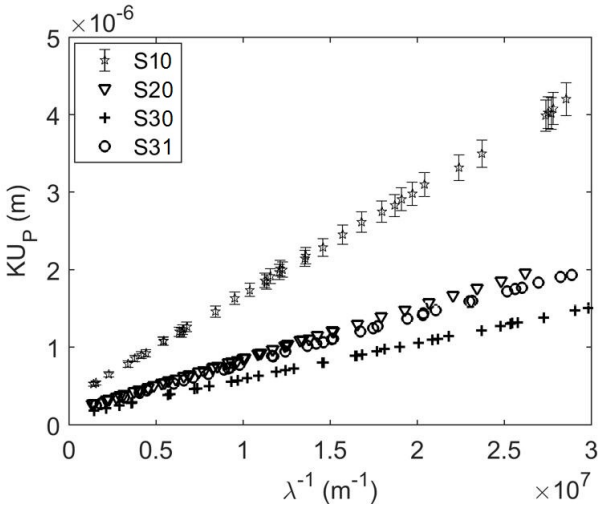

Figure 12: Characteristics curves for different membranes.

ϵ/τ^2, calculated with velocity slip coefficient, $\sigma_P = 1.016$, are summarized in Table 2, classified with an increasing hydraulic conductivity. The uncertainties are evaluated for fixed σ_P. Other reasonable values of the velocity slip coefficient for two gases used in experiments, Argon and Nitrogen, [17], $\sigma_P = 1.107 - 1.220$, would at most increase the estimation of pore radius for less than 20%. The measured pore radius (1.5 - 1.6 μm) does not change significantly between the different samples studied.

It is difficult to directly compare the results provided by gas flow method and those from mercury porosimetry

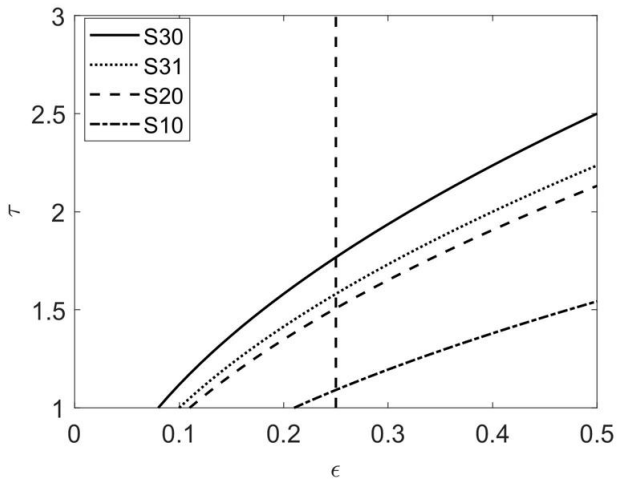

Figure 13: Tortuosity as a function of porosity for the different structure parameters measured.

or X-ray tomography. Indeed, the proposed gas flow method characterizes the whole fiber (3360 mm^3) while X-ray tomography or mercury porosimetry characterized a small volume of porous structure randomly sampled in the fiber (1-50 mm^3 respectively). Only orders of magnitude seem to be relevant to compare. The pore radius measured here is in reasonable agreement with result obtained by manufacturer with the mercury porosimetry, which is the reference characterization technique on the same type of sample ($\sim$ 1.5-3 µm).

Nevertheless, substantial variation, around 2.6 times, of the structure property coefficient ϵ/τ^2 are highlighted. A priori, it is impossible to know if the deviations between samples are due to variations of porosity, tortuosity or both simultaneously. According to the manufacturer's information, the possible variations in porosity from one sample to another are low. The reference value of porosity for this kind of porous media is around 25%.

Tortuosity values are plotted against porosity on Figure 13. Different values of tortuosity assuming the porosity equal to 25%, $\epsilon = 0.25$, are summarized in Table 2. According to various literature, predicting the tortuosity in porous media is difficult, in addition, the estimated values are strongly dependent on the model used. Nevertheless, a tortuosity over 4 seems very unlikely whatever model used [23, 24]. The values of tortuosity obtained from our measurements, varying as much as $1.1 < \tau < 1.8$, which is an acceptable range for a real porous material. The 3D reconstruction of this kind of hollow fiber based on X-ray tomography gives $\tau = 1.63$ [25].

Table 2: Fitting coefficients of the linear regression curve, eq. (16), characteristic pore radius, r, porous structure coefficient ϵ/τ^2 and value of tortuosity if the porosity is equal to 25%, for different porous media and the slip coefficient equal to 1.016.

	a(m^2) ±5%	b(m) ±5%	r(µm) ±10%	$\frac{\epsilon}{\tau^2}$ ± 15%	τ ± 15% for $\epsilon = 25\%$
S30	4.6×10^{-14}	1.2×10^{-7}	1.5	0.08	1.8
S31	6.2×10^{-14}	1.6×10^{-7}	1.6	0.10	1.6
S20	6.8×10^{-14}	1.7×10^{-7}	1.6	0.11	1.5
S10	13×10^{-14}	3.4×10^{-7}	1.6	0.21	1.1

5. Conclusion

A non-destructive method based on a gas flow in the "slip flow regime" was developed to measure the geometric characteristics of a microporous sample. The "slip flow" model, established and experimentally validated in the literature for a flow in a single microchannel, is extended to microporous media. This model allows the characterization of porous medium, crossed by the gas flow, by using two parameters. The first parameter is a representative characteristic dimension of the pore radius. The second characteristic is a dimensionless quantity corresponding to the ratio between porosity and squared tortuosity, ϵ/τ^2.

The proposed method is quite fast in experimental time: the characterization of a sample requires between $15-30$ minutes. It would be even faster with larger sample cross-section as the total mass flow rate would be higher for the same order of magnitude of the flows. The method was tested and validated on experimental data obtained with a set of ceramic membrane supports made using the same manufacturing procedure, but coming from three different batches. Similar characteristic pore radius was found for each of the tested samples. The same samples were measured using mercury porosimetry, which is the reference technique, but destructive for a sample, and the same characteristic pore radius was obtained for the same tested porous samples. However, the measurements show several differences between tested hollow fibers in terms of porous structure coefficient. Although the characteristic pore sizes are the same, the characterized samples exhibited different flow resistance. This behavior is expressed through the parameter ϵ/τ^2 which varies in an interval [0.08-0.21]. The proposed method allows us to experimentally distinguish between various samples, which were not previously known with conventional flow characterization techniques. Now it is also possible to give meaning to these differences between samples by referring to their geometrical characteristics, that of porosity and tortuosity.

Acknowledgments

This work is carried out in the framework of the ANR project MATEX 12-RMNP-0003.

References

[1] J. Sanz, R. Peinador, J. Calvo, A. Hernández, A. Bottino, G. Capannelli, Characterization of uf membranes by liquid liquid displacement porosimetry, Desalination 245 (1) (2009) 546 – 553, engineering with Membranes 2008. doi:https://doi.org/10.1016/j.desal.2009.02.019.
URL http://www.sciencedirect.com/science/article/pii/S0011916409003701

[2] S. ichi Nakao, Determination of pore size and pore size distribution: 3. filtration membranes, Journal of Membrane Science 96 (1) (1994) 131 – 165. doi:https://doi.org/10.1016/0376-7388(94)00128-6.
URL http://www.sciencedirect.com/science/article/pii/0376738894001286

[3] C. Causserand, G. Pierre, S. Rapenne, J.-C. Schrotter, P. Sauvade, O. Lorain, Characterization of ultrafiltration membranes by tracer's retention: Comparison of methods sensitivity and reproducibility, Desalination 250 (2) (2010) 767 – 772. doi:https://doi.org/10.1016/j.desal.2008.11.038.
URL http://www.sciencedirect.com/science/article/pii/S0011916409010376

[4] C. Cercignani, Mathematical methods in kinetic theory, Premuim Press, New York, London, 1990.

[5] T. Ewart, P. Perrier, I. Graur, J. Gilbert Méolans, Mass flow rate measurements in a microchannel, from hydrodynamic to near free molecular regimes, J. Fluid Mech. 584 (2007) 337–356. doi:10.1017/S0022112007006374.
URL http://dx.doi.org/10.1017/S0022112007006374

[6] G. el Hak M., The fluid mechanics of microdevices. the freeman scholar lecture, J. Fluids Eng. 121(1) (199) 5–33. doi:10.1115/1.2822013.
URL http://dx.doi.org/10.1115/1.2822013

[7] W.-M. Zhang, G. Meng, X. Wei, A review on slip models for gas microflows, Microfluidics and Nanofluidics 13 (6) (2012) 845–882. doi:10.1007/s10404-012-1012-9.
URL http://dx.doi.org/10.1007/s10404-012-1012-9

[8] T. Ewart, P. Perrier, I. Graur, J. Gilbert Méolans, Mass flow rate measurements in gas micro flows, Experiments in Fluids 41 (3) (2006) 487–498. doi:10.1007/s00348-006-0176-z.
URL http://dx.doi.org/10.1007/s00348-006-0176-z

[9] L. J. Klinkenberg, The permeability of porous media to liquids and gases., American Petroleum Institute.

[10] P. J. Rigden, The specific surface of powders. a modification of the theory of the air-permeability method, Journal of the Society of Chemical Industry 66 (4) (1947) 130–136. doi:10.1002/jctb.5000660407.
URL http://dx.doi.org/10.1002/jctb.5000660407

[11] R. S. Brodkey, H. C. Hershey, Transport phenomen : a unified approach, Mcgraw-Hill College, 1987.

[12] J. Pitakarnnop, S. Varoutis, D. Valougeorgis, S. Geoffroy, L. Baldas, S. Colin, A novel experimental setup for gas microflows, Microfluidics and Nanofluidics 8 (1) (2010) 57–72. doi:10.1007/s10404-009-0447-0.
URL http://dx.doi.org/10.1007/s10404-009-0447-0

[13] R. Schofield, A. Fane, C. Fell, Gas and vapour transport through microporous membranes. i. knudsen-poiseuille transition, Journal of Membrane Science 53 (1) (1990) 159 – 171. doi:http://dx.doi.org/10.1016/0376-7388(90)80011-A.
URL http://www.sciencedirect.com/science/article/pii/037673889080011A

[14] J. C. Arnell, G. O. Henneberry, Permeability studies: Iii. surface area measurements of carbon blacks, Canadian Journal of Research 26a (2) (1948) 29–38. arXiv:http://dx.doi.org/10.1139/cjr48a-004, doi:10.1139/cjr48a-004.
URL http://dx.doi.org/10.1139/cjr48a-004

[15] D. Wasan, M. Ranade, S. Sood, R. Davies, M. Jackson, B. Kaye, W. Wnek, Analysis and evaluation of permeability techniques for characterizing fine particles part ii. measurement of specific surface area, Powder Technology 14 (2) (1976) 229 – 244. doi:http://dx.doi.org/10.1016/0032-5910(76)80072-1.
URL http://www.sciencedirect.com/science/article/pii/0032591076800721

[16] C. Cercignani, Higher order slip according to the linearized Boltzmann equation, as-64-19 Edition, Berkeley : Institute of Engineering Research, University of California, 1964.

[17] P. Perrier, I. A. Graur, T. Ewart, J. G. Méolans, Mass flow rate measurements in microtubes: from hydrodynamic to near free molecular regime, Physic of fluids 23 (4).

[18] J. G. Méolans, M. H. Nacer, M. Rojas, P. Perrier, I. Graur, Effects of two transversal finite dimensions in long microchannel: Analytical approach in slip regime, Physics of Fluids 24 (11).

[19] L. Anez, S. Calas-Etienne, J. Primera, T. Woignier, Gas and liquid permeability in nano composites gels: Comparison of knudsen and klinkenberg correction factors, Microporous and Mesoporous Materials 200 (2014) 79 – 85. doi:http://dx.doi.org/10.1016/j.micromeso.2014.07.049.
URL http://www.sciencedirect.com/science/article/pii/S1387181114004156

[20] R. C. Johnson, Real gas effects in flow metering, Flow Its Measurement and Control in Science and Industry I (1974) 269–278.

[21] B. RASNEUR, J. CHARPIN, Caractérisation de la texture poreuse des matériaux base documentaire : TIB534DUO. (Archive / Réf : P1050 v1), fre. arXiv:basedocumentaire:TIB534DUO.
URL http://www.techniques-ingenieur.fr/base-documentaire/archives-th12/archives-techniques-d-analyse-tiata/archive-1/caracterisation-de-la-texture-poreuse-des-materiaux-p1050/

[22] Z. Zeng, R. Grigg, A criterion for non-darcy flow in porous media, Transport in Porous Media 63 (1) (2006) 57–69. doi:10.1007/s11242-005-2720-3.
URL http://dx.doi.org/10.1007/s11242-005-2720-3

[23] B. Ghanbarian, A. G. Hunt, R. P. Ewing, M. Sahimi, Tortuosity in porous media: A critical review, Soil Science Society of America Journal 77 (5) (2013) 1461–1477.

[24] M. Matyka, A. Khalili, Z. Koza, Tortuosity-porosity relation in porous media flow, Phys. Rev. E 78 (2008) 026306. doi:10.1103/PhysRevE.78.026306.
URL https://link.aps.org/doi/10.1103/PhysRevE.78.026306

[25] J.Perrin, J. Vicente, J. Bonnet, D. Borschneck, C. Savaro, P. Moulin, Morphological characterization of ceramic membranes from 3d x-ray computed tomography, in: Multi-scale Materials Under the Nanoscope, Paris (France), 2016.